An Untethered Miniature Origami Robot
that Self-folds, Walks, Swims, and Degrades

Shuhei Miyashita[1], Steven Guitron[1*], Marvin Ludersdorfer[2*], Cynthia R. Sung[1], and Daniela Rus[1]

Abstract— A miniature robotic device that can fold-up on the spot, accomplish tasks, and disappear by degradation into the environment promises a range of medical applications but has so far been a challenge in engineering. This work presents a sheet that can self-fold into a functional 3D robot, actuate immediately for untethered walking and swimming, and subsequently dissolve in liquid. The developed sheet weighs 0.31 g, spans 1.7 cm square in size, features a cubic neodymium magnet, and can be thermally activated to self-fold. Since the robot has asymmetric body balance along the sagittal axis, the robot can walk at a speed of 3.8 body-length/s being remotely controlled by an alternating external magnetic field. We further show that the robot is capable of conducting basic tasks and behaviors, including swimming, delivering/carrying blocks, climbing a slope, and digging. The developed models include an acetone-degradable version, which allows the entire robot's body to vanish in a liquid. We thus experimentally demonstrate the complete life cycle of our robot: self-folding, actuation, and degrading.

I. INTRODUCTION

There has been increasing demand for ubiquitous on-site construction of complex task-performing robotic devices lead by tidal progress in rapid and on-demand fabrication techniques. Such autonomous "4D-printed" robots could be used at unreachable sites, including those encountered in both in vivo and bionic biological treatment [1]. Although there are various methods for rapid fabrication of robot structures, a notable approach may be to construct a 3D structure by folding a 2D sheet with origami theory [2], [3], and to design the robots' bodies with the techniques [4]–[6]. Such composition methods, which can be referred to as "reconfiguration-based structuring," offer inexpensive and rapid manufacturing, as well as compact and lightweight transportation.

Different techniques have been investigated for self-folding planar materials, including shape memory alloy [7], [8] and shape memory polymer, with initiation by Joule heating [9], [10], electromagnetic waves [11], water on tracing paper [12], laser light emission on hydrogel [13], and residual tensile stress [14]. The self-folding technique that we have developed and used in the study employs heat to trigger deformation of shape memory polymer, which allows configuration of various structures [15]–[17] whose crease design can be made automatically [18], such as in self-assembling sensors [19], [20].
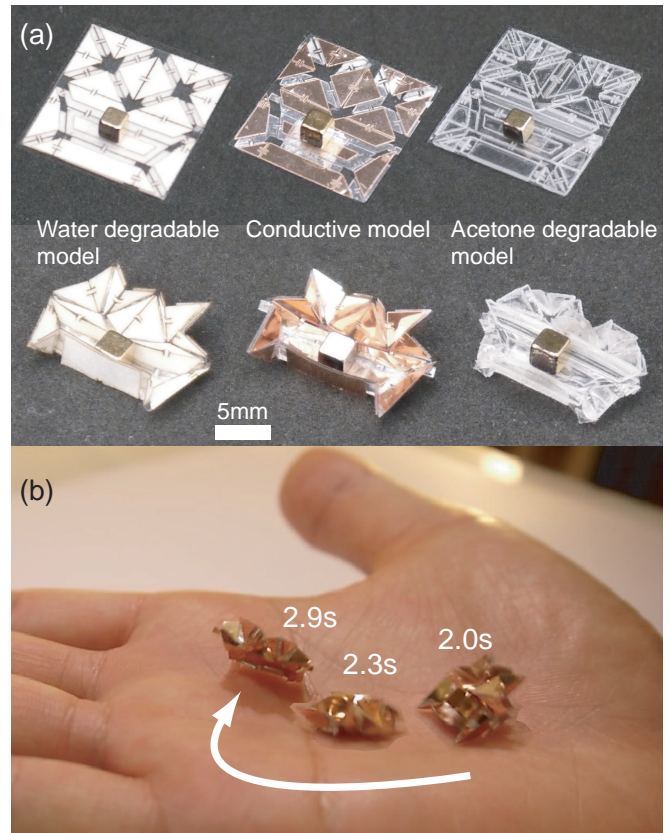
Fig. 1: The developed origami robot. (a) (From left to right) water-degradable model whose outer layer dissolves in water; conductive model (aluminum coated polyester); acetone-degradable model whose entire body (except magnet) dissolves in acetone. (b) Self-folded robot (controlled by a magnetic field) walking on a palm.

However, challenges include (I) how to reduce/eliminate integrated electronic parts, due to difficulty of both "printing" and removing the robot safely from the body should it be used in vivo; (II) how to actuate and control the robot despite reduced parts; and (III) how to "delete" the robot from the site after the robot has been used.

Here we address these issues in a mobile robot that can self-fold from a single planar material into a 3D structure that allows it to walk, swim, perform some basic tasks (such as block-pushing), and dissolve in liquid. In this paper, contributions include:

1) Performing on-site origami sheet self-folding followed by untethered actuation.
2) Developing the robot's control method for walking and

swimming using a newly developed electromagnetic system.

3) Testing the robot's ability to perform basic tasks and behaviors.

4) Demonstrating the robot's ability to degrade, as a proof of concept.

II. Robot Structure and Behavior Design

The goal for our robot is to self-reconfigure from a planar to a 3D structure, execute translational motion by walking and swimming, and vanish into the environment, all in series. To achieve this goal, we designed an on-stage self-folding technique (using global heating [15], [21] to catalyze the robot's reconfiguration), employed remote magnetic control for the robot's actuation, and utilized a specific material (polystyrene) for the robot's structure so that it could dissolve in a liquid (acetone). This section presents the robot's design and the actuation methods for both walking and swimming.

A. Force and Torque

The motion of the robot may vary depending on the desired application and environment of use, we aim for walking and swimming as basic capabilities. For a robot equipped with a magnet with magnetic dipole moment $\vec{m}$, the force $\vec{F}$ and torque $\vec{T}$ that the robot experiences in a magnetic flux density $\vec{B}$ are

$$\vec{F} = (\vec{m} \cdot \nabla)\vec{B}, \tag{1}$$
$$\vec{T} = \vec{m} \times \vec{B}, \tag{2}$$

where $\vec{B}$ is the globally created, superimposed magnetic flux density of all the coils in the environment. Assuming that the magnet's shape can be approximated as a sphere of radius a, $\vec{m}$ can be described with the saturation magnetization $\vec{M}_{sat}$ as

$$\vec{m} = \frac{4}{3}\pi a^3 \vec{M}_{sat}, \tag{3}$$

where M_{sat} is intrinsic to the material of the magnet. Torque is maximal when the relative angle between the magnet and the applied field reaches $90°$, and force is generated proportionally to the gradient of the magnetic field.

B. Robot's Design, Walking and Swimming Motion

The developed robot, which only weighs $0.31\,g$, is self-folded from the crease design shown in Fig. 2 (b) to the robot shown in Fig. 1 (a) and Fig. 2 (a). When heated, the structure folds up along the transverse plane and sagittal plane, bending in the middle of the shape similar to an inverted "V" along the sagittal plane. The frontal area forms the boat-shaped body which also functions as a support for the ground contact and the holding cage, while the back area forms two pivots (legs). The robot holds a magnet attached horizontally on the front side of the frontal plane placed equivalently high on the robot in relation to the center of mass of the body. This magnet's lifted positioning allows it to attain higher moment of inertia, and to stably move along the pitch and yaw axes in the air, induced by torque from the magnetic field.
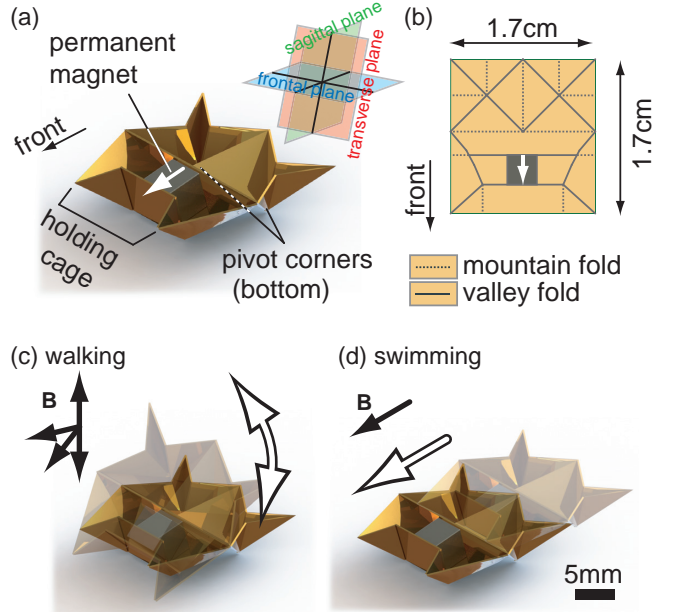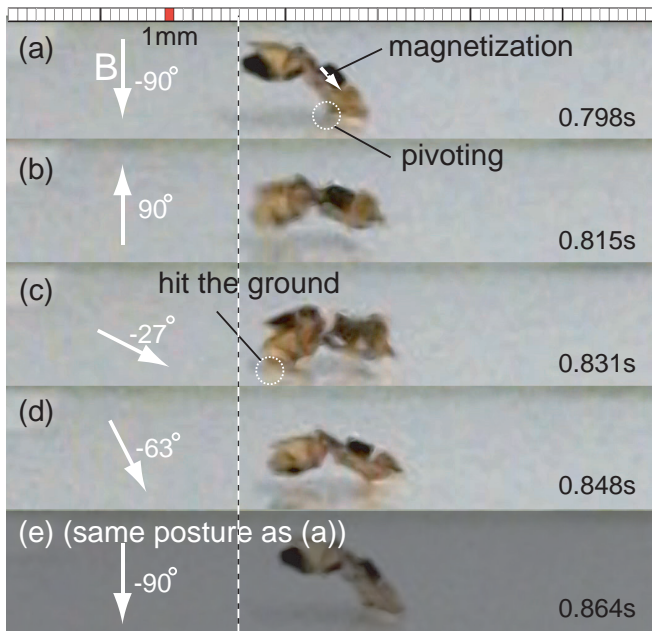

Fig. 2: The designed mobile robot and the actuation methods. (a) The outlook. (b) The crease pattern. (c) Walking mode by torque-based control. (d) Swimming mode by force-based control.

Walking is achieved by permitting the front and back body parts to alternately contact the ground as illustrated in Fig. 2 (c), where the off-centered body balance and the biased friction from the legs guarantee asymmetric body dynamics (moment of inertia) between front and back of the structure (see slow motion in Fig. 3). We apply an oscillatory constant magnitude magnetic field in the desired direction of motion with a rapid alternation of four states, namely $-27°$, $-63°$, $-90°$, and $90°$ at $15\,Hz$. Due to the friction from the front support and the frontal placement of the magnet, the transition from $-27°$ to $-63°$ to $-90°$ causes the robot to pivot about its front support. During the transition to $90°$, the applied torque causes the robot to rotate about the magnet, making it overcome the friction from the ground, and thrusting the robot forward. With this control, the robot can walk and turn, while the robot can hardly move in a sheet configuration. A comparable method can be found at a microscale level, known as stick-slip motion [22], where the method exploits a magnetic field gradient for control.

The robot also has a boat-shaped body so that it can float on water with roll and pitch stability. For swimming motion, a magnetic field gradient is applied in the direction of interest (Fig. 2 (d)). By setting coils that exert a magnetic field in the negative direction ($z < 0$) to a non-active state, this magnetic field gradient can be applied, and the magnet experiences force. In this way, the robot is capable of swimming forward and turning.

C. Self-folding and the Crease Generation Program

The self-folding sheet used in the study, capable of over 100 simultaneous bidirectional folds [15], [21], has a three layer structure, wherein a heat-sensitive contraction film (polyvinyl chloride; PVC) is sandwiched between two rigid
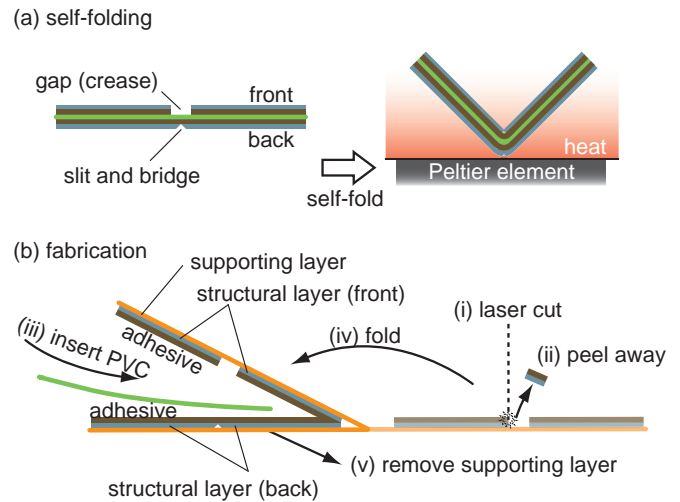
Fig. 3: One step of the walking motion taken by a high speed camera.

Fig. 4: Three layer structure for the heat-sensitive self-folding method. (a) Self-folding by global heat. (b) Fabrication process.

structural layers (Fig. 4 (a)). The self-folding crease patterns feature differentiated gap widths on the front and back face. When heated, the difference in the widths induces disproportionate contraction of PVC between the front and back faces at unmasked regions, causing a bending motion of the plane. When heat is applied to the structure from a Peltier element ($55 \times 55\,\mathrm{mm}^2$) situated below the structure, the exposed parts of the middle contraction layer shrink, causing a bending motion of the plane in the direction of the wider gap in the sheet. The non-exposed surfaces, covered by structural layers that sandwich both sides of the PVC, prevent the contraction of the PVC layer, and thus maintain their flat shape. After self-folding, the Peltier element helps to cool down the magnet, whose strength is weakened as temperature increases.

Fig. 4 (b) shows the fabrication process of a self-folding sheet. Once designed, the crease pattern is transformed into a mirrored front-and-back pattern laid side-by-side, using a programmed batch process. The generated new crease pattern is then etched onto structural and adhesive layers with a laser cutter machine (i). After the excessive components of the pattern have been stripped from the structural layer (ii), PVC film is placed between the front and the back forms of the crease pattern, and the two are pressed upon one another (iii-iv). Lastly, the supporting layer is removed (v). The whole process only requires a laser cutter machine for fabrication, but even the laser cutter can be substituted with an inexpensive vinyl cutter, thus making the process widely accessible.

III. MAGNETIC FIELD GENERATION

Remote magnetic actuation is a powerful approach mostly seen in the control of micro-sized magnets [22]–[29], as well as multiple magnets [30], [31]. This section introduces our electromagnetic coil system and explains how to apply current to obtain a targeted magnetic field for controlling the robot.

The system consists of four square electromagnetic coils inclined $45°$ from the horizontal plane, placed at regular intervals around the vertical axis in the lower half of a sphere of diameter d (Fig. 5). A local coordinate frame xyz is defined for each coil, such that the x-y plane is parallel to the surface of the coil, and z is normal to the surface, coinciding with the axis of symmetry of the coil. To simplify subsequent computations, the origin of the local coordinate frame is shifted, such that the centroid of the coil is located at $z = -d/2$, i.e., minus the radius of the sphere. The global coordinate frame XYZ is set with the origin at O, where the X and Y axes in the horizontal plane as visualized in Fig. 5. The work stage for the robot is placed at the intersection, just above the coils. This configuration leaves the upper half of the sphere open for the robot to operate.
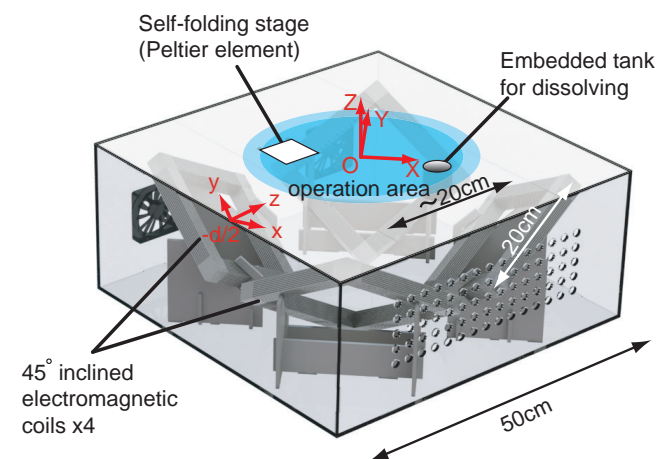
Fig. 5: The developed electromagnetic coil system.

The magnetic flux density generated around a conductive wire traversed by a current I can be calculated after the Biot-Savart law

$$\mathrm{d}\vec{b} = \frac{\mu_0 I}{4\pi} \frac{\mathrm{d}\vec{w} \times \hat{r}}{|\vec{r}|^2}, \tag{4}$$

where μ_0 is the vacuum permeability, $\mathrm{d}\vec{w}$ is an infinitesimal small segment of the wire, $\vec{r}$ is the vector pointing from $\mathrm{d}\vec{w}$ to the point of interest at which the magnetic flux density is to be calculated, and $\hat{r}$ is the unit vector pointing in that direction. Evaluating the contour integral over all infinitesimal segments of the wire gives the overall magnetic flux density generated at the point of interest [32]. Adapting this to the case of a square coil simplifies the contour integral to four line integrals [22]. Thus, the magnetic flux density $\vec{b}(x, y, z)$ generated at a position (x, y, z) relative to a coordinate frame associated with a square coil with N turns of side length D, traversed by a current I, is given by [22], [33]

$$\vec{b}(x, y, z) = \begin{pmatrix} b_x(x,y,z) \\ b_y(x,y,z) \\ b_z(x,y,z) \end{pmatrix} =$$

$$\frac{\mu_0 N I}{4\pi} \sum_{k=1}^{2} \sum_{l=1}^{2} \begin{pmatrix} (-1)^{k+l+1} \frac{(z-c)(y-y_l)}{r_{xy}} \frac{1}{r_x} \\ (-1)^{k+l+1} \frac{(z-c)(x-x_k)}{r_{xy}} \frac{1}{r_y} \\ (-1)^{k+l} \frac{(x-x_k)(y-y_l)}{r_{xy}} \left(\frac{1}{r_x} + \frac{1}{r_y} \right) \end{pmatrix}, \tag{5}$$

where $x_1 = y_1 = -D/2$, $x_2 = y_2 = D/2$,

$$r_{xy} := \sqrt{(x - x_k)^2 + (y - y_l)^2 + (z - c)^2},$$
$$r_x := (z - c)^2 + (x - x_k)^2,$$
$$r_y := (z - c)^2 + (y - y_l)^2,$$

and c is the position of the centroid of the coil along the z-direction of the coordinate frame. Here, $c = -d/2$.

The globally created magnetic flux density $\vec{B}(X, Y, Z)$ is given by the superposition of the individual magnetic flux densities $\vec{b}_L(X, Y, Z)$ generated by the four electromagnets, expressed in global coordinates. That is,

$$\vec{B}(X, Y, Z) = \sum_{L=1}^{4} \vec{b}_L(X, Y, Z). \tag{6}$$

To derive each individual $\vec{b}_L(X, Y, Z)$, (5) has to be rotated to match the orientation of the respective coil relative to the global coordinate frame, as depicted in Fig. 5. Furthermore, a coordinate transform has to be introduced to express each local coordinate set in the global coordinates. This yields

$$\vec{b}_L(X, Y, Z) = R_L \vec{b}(x_L, y_L, z_L), \quad L = 1, \dots, 4. \tag{7}$$

The four 3×3 rotation matrices $R_L := R(\alpha)$, where $\alpha \in \{0, \pi/2, \pi, 3\pi/2\}$ describes the orientation of the local frame with respect to the global one [34], are given by

$$R(\alpha) = \begin{bmatrix} \frac{\cos\alpha}{2} + \frac{\sin\alpha}{\sqrt{2}} & \frac{\cos\alpha}{2} - \frac{\sin\alpha}{\sqrt{2}} & -\frac{\cos\alpha}{\sqrt{2}} \\ \frac{\sin\alpha}{2} - \frac{\cos\alpha}{\sqrt{2}} & \frac{\sin\alpha}{2} + \frac{\cos\alpha}{\sqrt{2}} & -\frac{\sin\alpha}{\sqrt{2}} \\ \frac{1}{2} & \frac{1}{2} & \frac{1}{\sqrt{2}} \end{bmatrix}. \tag{8}$$

With these, the coordinate transform becomes

$$\begin{pmatrix} x_L \\ y_L \\ z_L \end{pmatrix} = R_L^{-1} \begin{pmatrix} X \\ Y \\ Z \end{pmatrix}. \tag{9}$$

Relation (6) is linear in the currents I_L and therefore can be rewritten as

$$\vec{B}(X, Y, Z) = J(X, Y, Z)\,\vec{I}, \tag{10}$$

where $J(X, Y, Z)$ is a 3×4 Jacobian matrix relating current $\vec{I}$ to magnetic flux density $\vec{B}(X, Y, Z)$.

One solution for the current $\vec{I}$ required to generate a desired magnetic flux density $\vec{B}(X, Y, Z)$ at the stage can be determined by solving the unconstrained least squares problem

$$\underset{\vec{I}}{\text{minimize}} \ \|J(X, Y, Z)\,\vec{I} - \vec{B}(X, Y, Z)\|_2 \tag{11}$$

corresponding to the underdetermined system of equations (10). The least squares problem (11) can for instance be solved using the Moore-Penrose pseudo inverse of the Jacobian matrix J

$$\vec{I} = J^{\#}\vec{B}, \quad J^{\#} = J^T(JJ^T)^{-1}, \tag{12}$$

where the position dependence of $J(X, Y, Z)$ and $\vec{B}(X, Y, Z)$ has been omitted for clarity. This minimizes the Euclidean norm of $\vec{I}$, thereby minimizing both energy consumption and heat generation [27].

The torque $\vec{T}$ acting on a magnet due to $\vec{B}(X, Y, Z)$ can be calculated from (2). The 3×3 skew-symmetric matrix corresponding to $\vec{m} := (m_X \, m_Y \, m_Z)^T$ defined in (3) allows the cross product in (2) to be expressed as a matrix multiplication. That is,

$$\vec{T} = \begin{bmatrix} 0 & m_Z & -m_Y \\ -m_Z & 0 & m_X \\ m_Y & -m_X & 0 \end{bmatrix} \vec{B}(X, Y, Z). \tag{13}$$

With (10) follows that $\vec{T}$ is linear in the currents $\vec{I}$. Therefore the previous equation can be rewritten as

$$\vec{T} = J_T(X, Y, Z)\,\vec{I}, \tag{14}$$

where $J_T(X, Y, Z)$ is a 3×4 Jacobian matrix relating current $\vec{I}$ to torque $\vec{T}$.

The force $\vec{F}$ acting on a magnet due to $\vec{B}(X, Y, Z)$ can be calculated from (1). With equations (13.47a and b) from [35] follows
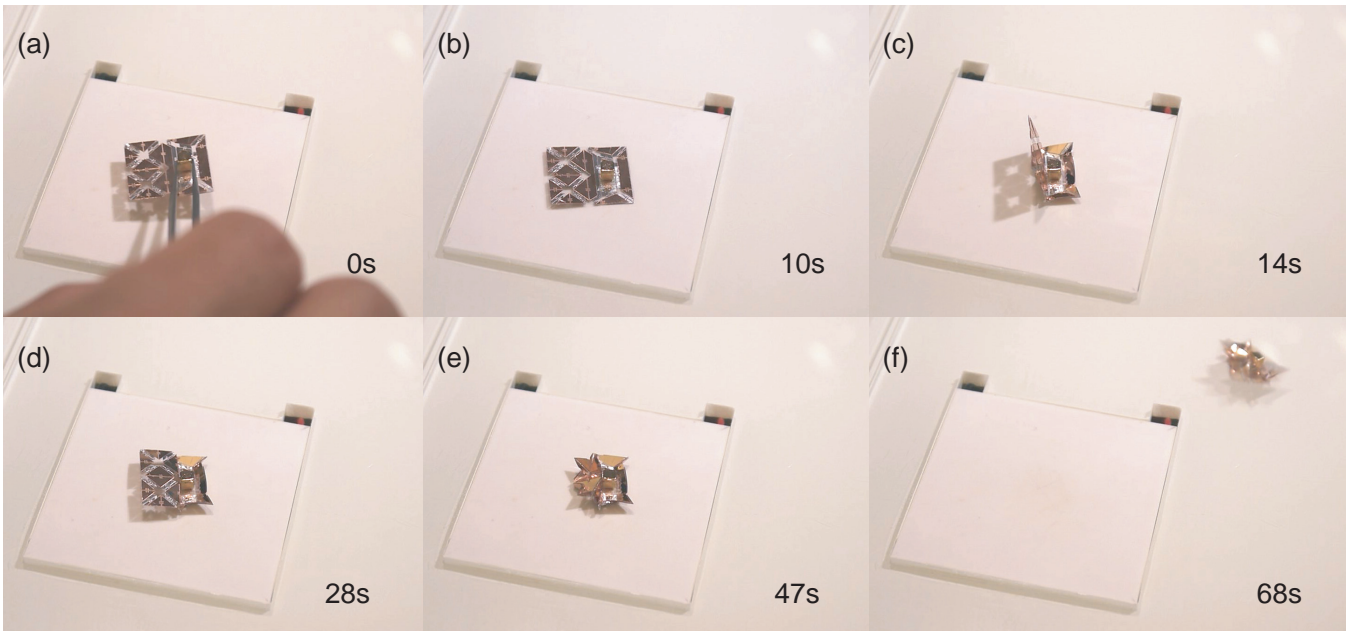
$$\vec{F} = \begin{bmatrix} \frac{\partial \vec{B}(X,Y,Z)}{\partial X} & \frac{\partial \vec{B}(X,Y,Z)}{\partial Y} & \frac{\partial \vec{B}(X,Y,Z)}{\partial Z} \end{bmatrix} \vec{m}, \tag{15}$$

where $\vec{m}$ as defined in (3). Therefore, $\vec{F}$ is linear in the currents $\vec{I}$ and can be rewritten as

$$\vec{F} = J_F(X, Y, Z)\,\vec{I}, \tag{16}$$

where $J_F(X, Y, Z)$ is a 3×4 Jacobian matrix relating current $\vec{I}$ to force $\vec{F}$. With (14) and (16) follows

$$\begin{pmatrix} \vec{T} \\ \vec{F} \end{pmatrix} = \underbrace{\begin{bmatrix} J_T(X, Y, Z) \\ J_F(X, Y, Z) \end{bmatrix}}_{:=A(X,Y,Z)} \vec{I} = A(X, Y, Z)\,\vec{I}, \tag{17}$$

Fig. 6: Proof of concept of self-folding and immediate actuation of the robot. (a) Placement. (b)-(e) Self-folding. (f) Walking, all done in sequence without physical intervention of an operator. See the attached video.

where $A(X, Y, Z)$ is a 6×4 actuation matrix describing the torque and force acting on a magnet inside the area of operation due to the currents applied to the four electromagnetic coils [27].

With this coil arrangement, the system is capable of generating a magnetic field in an arbitrary direction at a location sufficiently close to the center of the sphere. A uniform field is guaranteed with arbitrary strength along the X-Y plane, with a non-uniform field along the Z-direction. When a generated magnetic field only has X and Y components, a magnet lying on the $X - Y$ plane can turn while keeping its position (yaw motion). By including a magnetic field component in the Z-direction, the magnet can also face upwards (pitch motion), pivoting up from the ground.

In the developed system, a magnetic field with a strength of $0.6 \, \text{mT}$ was measured in the Z-direction at point O with a total current flow of $10 \, \text{A}$ ($\sim 100 \, \text{W}$). This magnetic field strength almost matched what was estimated with the model. A robot can be stably actuated within a circle of diameter $\sim 20 \, \text{cm}$, which is called the "operation area", by employing rectangular coils of $D = 20 \, \text{cm}$. This operation area could be scaled up by employing the relationship found in (6). Given that c is to be increased while $\vec{B}$ should remain unchanged, N, D and $\vec{I}$ need to be adapted according to (5).

The X-Y direction of the magnetic field was controlled by the joystick on an Arduino Esplora, whose MCU handles all of the computation. Current was drawn from a power supply, and commands were transferred from the MCU to four SyRen 10 motor drivers (Dimension Engineering) through packetized serial communication in real time. Heating and cooling the Peltier element, switching between walking and swimming modes, and changing the magnitude of the mag-

netic field can all be controlled by either pressing a button or adjusting the slider on the Arduino Esplora controller. The robot can also move from land to water by changing the mode from torque-based walking to drag-based swimming.

## IV. RESULTS

A. Self-folding and Immediate Action

We demonstrated on-stage self-folding as well as immediate actuation and showed the result as snapshots in Fig. 6, as a proof of concept. After about $10 \, \text{s}$ from its placement (Fig. 6 (a)), the sheet started to self-fold at around $65°\text{C}$ (Fig. 6 (b)) beginning with longer creases that received thermal energy faster than the other creases (Fig. 6 (c)-(d)). The transformation was completed in about one minute (Fig. 6 (e)). The self-folded robot was actuated immediately without human intervention after a short period of cooling down (Fig. 6 (f)).

This integrated process shows that a functional structure can be produced from a planar material and instantly be employed for task operations.

B. Task Performances

The robot can complete various tasks due to its mobile characteristics. This section presents some examples of such actions, controlled with a joystick. The robot can walk in a figure "8" pattern (Fig. 7 (a)), float and swim on water (Fig. 7 (b)), push and deliver a lightweight block (Fig. 7 (c)), carry two times $(0.614 \, \text{g})$ its weight $(0.31 \, \text{g})$ (Fig. 7 (d)), climb a slope of $8.5°$ (Fig. 7 (e)), walk on rough terrain (Fig. 7 (f), see also Fig. 1 (b)), and dig into a stack of sponges (Fig. 7 (g)).

During experiments, while the robot's walking dynamics maintained stability, the robot often unexpectedly flipped
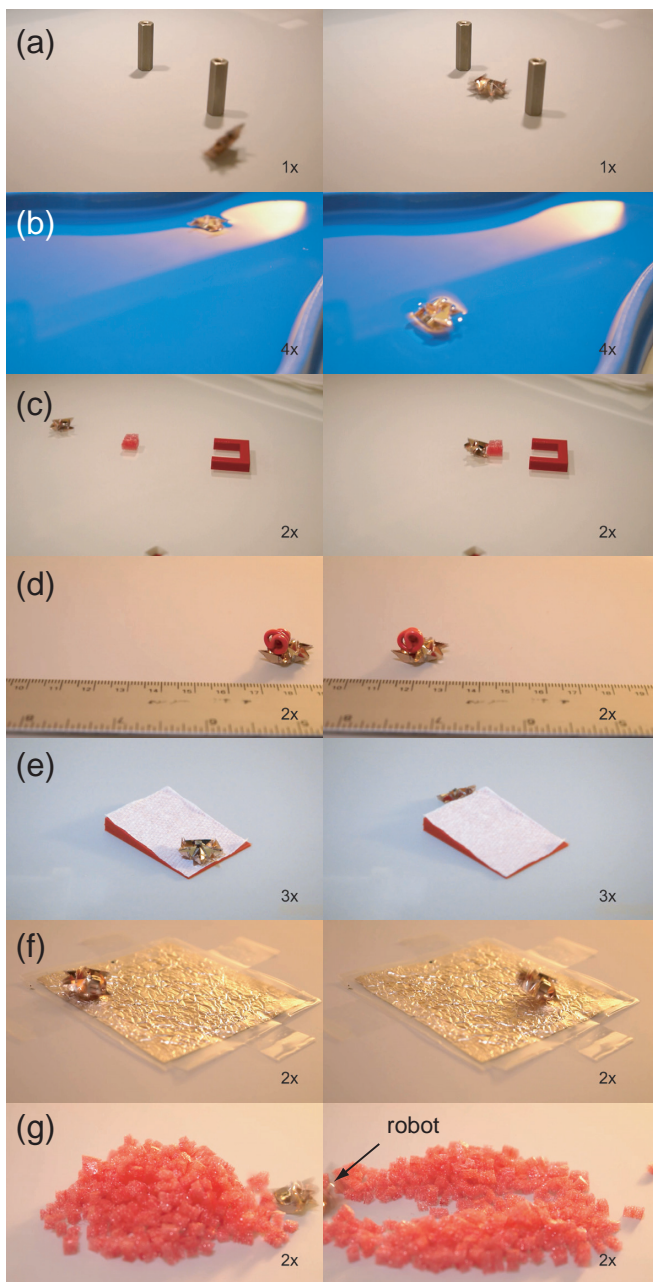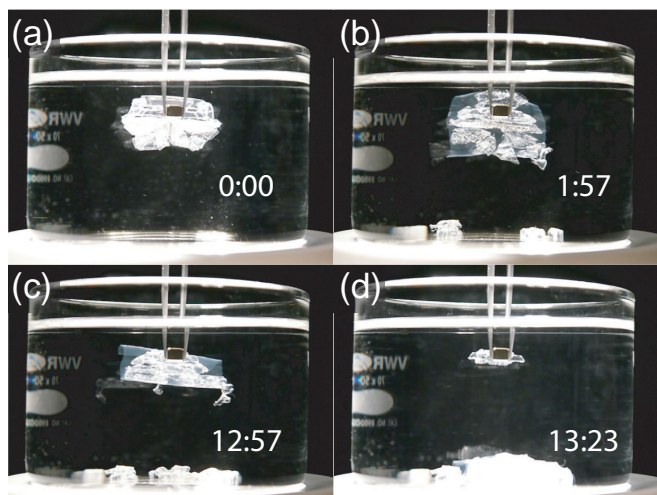
Fig. 7: Performances. (a) Walking on a trajectory. (b) Swimming. (c) Block delivery. (d) Carrying a load. (e) Climbing a slope. (f) Walking on rough terrain. (g) Digging through a stack. See the attached video.

Fig. 8: Polystyrene model robot that dissolves in acetone. See the attached video.

over. This flip happened particularly when the robot suddenly changed its walking direction to 180° opposite the original trajectory. Such instability can be avoided by restricting the change of the robot's motion. The robot can recover the original posture by receiving an impulsive asymmetric magnetic field.

C. Concept of Degradable Robots

This section demonstrates the degrading process of two developed robots: (I) one whose entire body except for the magnet can dissolve in acetone, and (II) one whose outer layer (structural layer) dissolves in water. For the first, we chose acetone for the liquid solution due to the use of PVC in the structure and made the structural layer out of polystyrene. These degradable models proved to be as controllable and versatile as the original conductive model in the experiments.

The time lapse snapshots show that all materials (polystyrene, PVC film, and silicone adhesive) that compose the robot dissolve into acetone, although there are time differences in the reaction speeds between the materials (i.e., compared to the body material made of polystyrene, PVC, which can be seen in Fig. 8 (d), took longer time to dissolve). Polystyrene also has a drawback due to its relatively low melting temperatures (∼ 70°C), close to the temperatures required for self-folding. This demonstration completes our scenario in which a robot can be instantiated by self-folding, immediately employed for accomplishing tasks, and erased on the spot without human physical intervention.

The dissolving process of the water-degradable model was tested under the assumption that future advancements would make the model biodegradable. Unlike the acetone-degradable model, the water-degradable model required stirring for enhanced segregation of the materials. A structure without the outer layer was obtained after about 3 minutes (not in the figure). To construct a biodegradable model for clinical use, the contraction layer (PVC film) and the adhesive layer need to be replaced with biodegradable counterparts.

V. DISCUSSION & CONCLUSION

In this paper, we present a novel single-sheet structure that self-folds into a centimeter-sized mobile robot that subsequently walks, swims, and dissolves. The robot is controlled using an external magnetic field exerted by embedded coils underneath the robot. Equipped with just one permanent magnet, the robot features a lightweight body yet can perform many tasks reliably despite its simplicity. The minimal body materials enable the robot to completely dissolve in a liquid environment, a difficult challenge to accomplish if

the robot had a more complex architecture. This study is the first to demonstrate that a functional robotic device can be created and operated from the material level, promising versatile applications including use in vivo. Our future work involves combining the conductive robot body with self-folding sensors [20] to achieve a higher level of autonomy and more versatility in function.

ACKNOWLEDGMENT

REFERENCES

[1] D. D. Damian, S. Arabagi, A. Fabozzo, P. Ngo, R. Jennings, M. Manfredi, and P. E. Dupont, "Robotic implant to apply tissue traction forces in the treatment of esophageal atresia,," in *IEEE International Conference on Robotics and Automation (ICRA)*, 2014, pp. 786–792.

[2] R. J. Lang, *Origami Design Secrets*. CRC Press, Taylor & Francis Group, 2012.

[3] Z. Abel, E. D. Demaine, M. L. Demaine, S. Eisenstat, A. Lubiw, A. Schulz, D. L. Souvaine, G. Viglietta, and A. Winslow, "Algorithms for Designing Pop-Up Cards," in *30th International Symposium on Theoretical Aspects of Computer Science (STACS 2013)*, vol. 20, 2013, pp. 269–280.

[4] A. M. Hoover, E. Steltz, and R. S. Fearing, "RoACH: An autonomous 2.4g crawling hexapod robot," in *IEEE/RSJ International Conference on Intelligent Robots and Systems (IROS)*, 2008, pp. 26–33.

[5] J. P. Whitney, P. S. Sreetharan, K. Ma, and R. J. Wood, "Pop-up book MEMS," *Journal of Micromechanics and Microengineering*, vol. 21, no. 11, p. 115021, 2011.

[6] C. D. Onal, R. J. Wood, and D. Rus, "Towards printable robotics: Origami-inspired planar fabrication of three-dimensional mechanisms," in *IEEE International Conference on Robotics and Automation (ICRA)*, 2011, pp. 4608–4613.

[7] E. Hawkes, B. An, N. M. Benbernou, H. Tanaka, S. Kim, E. D. Demaine, D. Rus, and R. J. Wood, "Programmable matter by folding," *Proceedings of the National Academy of Sciences*, vol. 107, no. 28, pp. 12 441–12 445, 2010.

[8] A. Firouzeh, Y. Sun, H. Lee, and J. Paik, "Sensor and actuator integrated low-profile robotic origami," in *IEEE/RSJ International Conference on Intelligent Robots and Systems (IROS)*, 2013.

[9] S. M. Felton, M. T. Tolley, C. D. Onal, D. Rus, and R. J. Wood, "Robot self-assembly by folding: A printed inchworm robot," in *IEEE International Conference on Robotics and Automation (ICRA)*, 2013, pp. 277–282.

[10] S. Felton, M. T. Tolley, E. Demaine, D. Rus, and R. J. Wood, "A method for building self-folding machines," *Science*, vol. 345, pp. 644–646, 2014.

[11] K. Yasu and M. Inami, "Popapy: instant paper craft made up in a microwave oven," in *The 9th International Conference on Advances in Computer Entertainment*, 2012.

[12] C. Guberan. (2012). [Online]. Available: http://vimeo.com/39914902

[13] S. Fusco, M. S. Sakar, S. Kennedy, C. Peters, R. Bottani, F. Starsich, A. Mao, G. A. Sotiriou, S. Pan, S. E. Pratsinis, D. Mooney, and B. J. Nelson, "An integrated microrobotic platform for on-demand, targeted therapeutic interventions," *Advanced Materials*, vol. 26, p. 952957, 2013.

[14] N. Bassik, G. M. Stern, and D. H. Gracias, "Microassembly based on hands free origami with bidirectional curvature," *Applied Physics Letters*, vol. 95, pp. 091 901–1–091 901–3, 2009.

[15] S. Miyashita, C. D. Onal, and D. Rus, "Self-pop-up cylindrical structure by global heating," in *IEEE/RSJ International Conference on Intelligent Robots and Systems (IROS)*, 2013.

[16] M. T. Tolley, S. M. Felton, S. Miyashita, D. Aukes, D. Rus, and R. J. Wood, "Self-folding origami: shape memory composites activated by uniform heating," *The IOP Journal Smart Materials and Structures*, vol. 23, p. 094006, 2014.

[17] S. Miyashita, I. DiDio, I. Ananthabhotla, B. An, C. Sung, S. Arabagi, and D. Rus, "Folding angle regulation by curved crease design for self-assembling origami propellers," *Journal of Mechanisms and Robotics*, 2015, doi:10.1115/1.4029548.

[18] B. An, S. Miyashita, M. T. Tolley, D. M. Aukes, L. Meeker, E. D. Demaine, M. L. Demaine, R. J. Wood, and D. Rus, "An end-to-end approach to making self-folded 3d surface shapes by uniform heating," in *IEEE International Conference on Robotics and Automation (ICRA)*, 2014, pp. 1466–1473.

[19] S. Miyashita, L. Meeker, M. Göldi, Y. Kawahara, and D. Rus, "Self-folding printable elastic electric devices: Resistor, capacitor, and inductor," in *IEEE International Conference on Robotics and Automation (ICRA)*, 2014, pp. 1446–1453.

[20] S. Miyashita, L. Meeker, M. Göldi, M. T. Tolley, R. J. Wood, and D. Rus, "Self-folding miniature elastic electric device," *The IOP Journal Smart Materials and Structures*, vol. 23, p. 094005, 2014.

[21] S. Miyashita, C. D. Onal, and D. Rus, "Multi-crease self-folding by global heating." *To appear in Artificial Life Journal*.

[22] S. Floyd, C. Pawashe, and M. Sitti, "Modeling and experimental characterization of an untethered magnetic micro-robot." *The International Journal of Robotics Research*, vol. 28, pp. 1077–1094, 2009.

[23] T. Honda, K. I. Arai, and K. Ishiyama, "Micro swimming mechanijsms propelled by external magnetic fields," *IEEE Transactions on Magnetics*, vol. 32, pp. 5085–5087, 1996.

[24] K. Ishiyama, M. Sendoh, and K. Arai, "Magnetic micromachines for medical applications," *Journal of Magnetism and Magnetic Materials*, vol. 242-245, pp. 41–46, 2002.

[25] S. Martel, J.-B. Mathieu, O. Felfoul, A. Chanu, E. Aboussouan, S. Tamaz, P. Pouponneau, L. Yahia, G. Beaudoin, G. Soulez, and M. Mankiewicz, "Automatic navigation of an untethered device in the artery of a living animal using a conventional clinical magnetic resonance imaging system," *Applied Physics Letters*, vol. 90, p. 114105, 2007.

[26] K. Vollmers, D. R. Frutiger, B. E. Kratochvil, and B. J. Nelson, "Wireless resonant magnetic microactuator for untethered mobile microrobots," *Applied Physics Letters*, vol. 92, no. 14, 2008.

[27] M. P. Kummer, J. J. Abbott, B. E. Kratochvil, R. Borer, A. Sengul, and B. J. Nelson, "Octomag: An electromagnetic system for 5-dof wireless micromanipulation," in *IEEE International Conference on Robotics and Automation (ICRA)*, 2010, pp. 1006–1017.

[28] S. Miyashita, E. Diller, and M. Sitti, "Two-Dimensional Magnetic Micro-module Reconfigurations Based on Inter-modular Interactions," *International Journal of Robotics Research*, vol. 32, pp. 591–615, 2013.

[29] E. Diller, J. Giltinan, G. Z. Lum, Z. Ye, and M. Sitti, "Six-degrees-of-freedom remote actuation of magnetic microrobots," in *Robotics: Science and Systems Conference*, 2014.

[30] B. E. Kratochvil, D. R. Frutiger, K. Vollmers, and B. J. Nelson, "Visual servoing and characterization of resonant magnetic actuators for decoupled locomotion of multiple untethered mobile microrobots," in *Proc. IEEE International Conference on Robotics and Automation (ICRA), Kobe, Japan*, May 2009, pp. 1010 – 1015.

[31] E. Diller, J. Giltinan, and M. Sitti, "Independent control of multiple magnetic microrobots in three dimensions," *International Journal of Robotics Research*, vol. 32, no. 5, pp. 614–631, 2013.

[32] P. A. Tipler and G. Mosca, *Physics for Scientists and Engineers*, 6th ed. Palgrave Macmillan.

[33] W. M. Frix, G. G. Karady, and B. A. Venetz, "Comparison of calibration systems for magnetic field measurement equipment," *IEEE Transactions on Power Delivery*, vol. 9, no. 1, pp. 100–108, 1994.

[34] W. Khalil and E. Dombre, *Modeling, Identification & Control of Robots*. Hermes Penton Science, 2002.

[35] I. N. Bronshtein, K. A. Semendyayev, G. Musiol, and H. Mühlig, *Handbook of Mathematics*, 5th ed. Springer-Verlag Berlin Heidelberg, 2007.